Journal of Physics D: Applied Physics

Photoluminescence intensity of Cu-doped ZnO modulated via defect occupancy by applying electric bias

To cite this article before publication: Lok Ping Ho *et al* 2022 *J. Phys. D: Appl. Phys.* in press https://doi.org/10.1088/1361-6463/ac6912

Photoluminescence intensity of Cu-doped ZnO modulated via defect occupancy by applying electric bias

Lok-Ping Ho[1], Muhammad Younas[2], Jon Borgersen[3], Rao Tahir Ali Khan[4], Seyed Javad Rezvani[5], Simone Pollastri[6], Muhammad Javed Akhtar[4], Muhammad Nadeem[2], Dong Huang[1], Ying-Li Shi[1], Andrej Kuznetsov[3*], Francis Chi-Chung Ling[1*]

[1] Department of Physics, The University of Hong Kong, Pokfulam, Hong Kong, China
E-mail: ccling@hku.hk

[2] PCG, Physics Division, PINSTECH, P.O. Nilore, Islamabad 45650, Pakistan

[3] Department of Physics and Centre for Material Science and Nanotechnology, University of Oslo, N-0318 Oslo, Norway
E-mail: andrej.kuznetsov@fys.uio.no

[4] Physics Division, PINSTECH, P.O. Nilore, Islamabad 45650, Pakistan

[5] CNR-IOM Lab TASC Area Science Park, Basovizza Building MM, 34149, Trieste, Italy

[6] Elettra S.S. 14, Km 163.5 in Area Science Park, Basovizza 34149, Italy

Keywords: multifunctional materials, luminescence modulation, resistive switching, X-ray absorption spectroscopy, defects, ZnO

Discovering multifunctional materials is of paramount importance for advancing the science and technology. Herein, we report on an optical phenomenon modulated by an electrical process that happened at the metal-ZnO:Cu junction, for which the light emission intensity from the photoluminescence is tuned reversibly by applying electric bias to the junction. Importantly, these observations were correlated with the x-ray absorption measurements, detecting prominent flips in Cu^{+}/Cu^{2+} oxidation state occupations in ZnO:Cu film as a function of the resistive switching. Moreover, further analysis of the x-ray absorption data revealed an additional prominent correlation - the signals interpreted as the Zn-O bond fingerprints also exhibited the modulations. By considering the whole set of data, we proposed a scenario explaining the modulation phenomena.

1. Introduction

Discovering multifunctional materials is of paramount importance for advancing the science and technology. In particular, manipulating light by non-optical phenomena is interesting for the fundamental physics development and for fabricating novel devices. Indeed, there are excellent demonstrations interconnecting light and applied electric field, e.g. in light emitting diodes – featuring a great scientific success and continuously entering new cross-disciplinary markets.[1] Moreover, the interplay between a magnetic field and light, e.g. in the form of magnetoluminescence, is also known,[2] even though it has not yet resulted in similarly prominent applications.

More specifically, the magnetic and optical properties of materials may be controlled by changing the resistance state in the memristors. For example, switching of the resistance of the metal/ZnO:Cu structure by applying a positive bias and negative bias were reported and this phenomenon was termed resistive switching [3-7]. Using this material, Younas et al.[8] observed interesting magnetic switching, so that the saturation magnetization was significantly reduced, while switching the memristor from the high resistance state (HRS) to the low resistance state (LRS). Thus, the resistive switching is an interesting option for controlling other physical properties of materials, providing additional opportunities for device functionalization. Controlled by applying electric bias, He et al.[9] reported prominent emission peak shifts of graphene/SiO_2 based structures, and Yang et al.[10] reported electroluminescence intensity modulations from Au/GaO_x/p-GaN/n-ZnO light emitting diode structures.

Although there are reports on modulation of luminescence by applying electric bias, there was little effort devoted to understand the physics behind the phenomenon. In the present study, we observed photoluminescence (PL) intensity modulation on the metal/ZnO:Cu structure by applying positive and reverse bias. Importantly, the PL observations were correlated with the x-ray absorption measurements, detecting prominent flips in Cu^{+}/Cu^{2+}

oxidation state occupations in the ZnO:Cu film as a function of the luminescence intensity modulation. Moreover, the analysis of the Zn K-edge x-ray absorption fine structure spectra indicated an additional prominent correlation - the signals interpreted as the Zn-O bond fingerprints also exhibited modulations. By considering the whole data set, we proposed a consistent scenario explaining the modulation phenomena.

5. Experimental Methods

The active part of the Al/ZnO:Cu/ZnO:Ga/Al_2O_3 memristor structure was fabricated by pulsed laser deposition (PLD)[8,11]. Specifically, the ZnO:Cu/ZnO:Ga sandwich structures were fabricated by PLD on single crystalline c-axis oriented Al_2O_3 substrates (purity >99.996%), as supplied from Crystal-Optech Co. Ltd. The background pressure in the PLD system was 10^{-4} Pa. During the growth, the oxygen pressure P(O_2) and the substrate temperature were kept at 0.02 Pa and 600 ^oC, respectively. The ZnO:Cu and ZnO:Ga films were fabricated using the ZnO:CuO (Cu=4 wt%, purity=99.999%) and ZnO:Ga_2O_3 (Ga=1 wt%, purity=99.999 %) ceramics targets, respectively. A 248 nm wavelength KrF excimer laser, having a pulse energy of 300 mJ and a repetition rate of 2 Hz was used to ablate the targets. The ZnO:Cu film was ~300 nm thick. The conductive ZnO:Ga (GZO) film was ~50 nm thick, exhibiting ~90% optical transmission in the visible range and resistivity of ~1×10^{-4} Ω. A part of the GZO film was masked prior to the ZnO:Cu film deposition, providing sufficient area for making ohmic contact on the GZO film. This GZO film with an ohmic contact formed the backside electrode. Finally, the front side Al contacts were fabricated on top of the ZnO:Cu/GZO sandwich by e-beam evaporation through a mask, resulting in the 4x4 array of circular Al contacts, 0.25 mm in diameter, separated by 0.25 mm. Thus, we can differentiate between the individual components, each with its own Al top contact, and the whole memeristor cell or device – encompassing the 4x4 array of the individual components. The inset in Fig.1 shows the schematics of the device.

The electrical characterization was monitored by current-voltage (*IV*) measurements using a Keithley 2601B setup at room temperature (RT). Initially, the *IV* characteristics were measured in the range from –4V to +4V. The voltage ($V_{applied}$) was applied to the front side Al electrode, always keeping the backside GZO electrode at 0V. It was found (see Sec.3 for details) that applying bias of –4V and +4V set the sample resistance to the states of high resistance and low resistance (denoted respectively by HRS and the LRS). The resistive state of the sample after setting to HRS or LRS and then unwired were tested by a small testing voltage (+0.5 V, referred to the monitoring IV measurement for the rest of the paper). The sample resistance after set to HRS and LRS are non-volatile, meaning that the sample resistance measured by a small testing voltage persisted after the sample was set and unwired. Notably, all the 4x4 Al/ZnO:Cu/GZO components were tested individually, showing very similar resistive switching magnitude in multiple tests; the same performance was observed if switching the 4x4 device array as a whole.

The PL was measured both at room temperature and at 10K, after setting the samples to the HRS and LRS electrically and unwired. The PL study was conducted on the front side of the sample with the excitation laser illuminating at the bare area in-between the Al electrode. A Kimmon He-Cd continuous laser was used as excitation source, keeping the power at 30 mW. The PL excitation and the data collection were performed from the front side of the sample. The PL spectra were collected by a monochromator with a focal length of 500 mm, a photomultiplier tube and a lock-in amplifier (Omni-λ 5008 system). For the 10K PL measurements, an Oxford Instrument closed cycle He refrigerator was used. The spot size of the PL excitation beam was ~1 mm on the sample. The beam incidence was aligned with the center of the device, so that the PL signal was collected from the device volume correlated with at least 4 central individual Al/ZnO:Cu/GZO components. Importantly, all 4x4 components of the device were set consequently at HRS/LRS to record the corresponding PL modulations.

Notably, several batches of devices were fabricated on similarly synthesized wafers; these devices demonstrated very similar patterns for the PL modulation and switching states.

The x-ray absorption spectra (XAS) were acquired at RT after switching the samples to the HRS and LRS. The data were obtained from the front side of the samples at the ELETTRA Synchrotron (Trieste, Italy) with the storage ring running at 2GeV and a typical current of 300mA. The Cu-$L_{3/2}$ edge X-ray absorption near edge structure (XANES) data were collected at the BL8.1L station of the ELETTRA. The spectral energy was calibrated by referring to C $1\pi - 1\pi*$ transitions. The incident light was horizontally polarized and the incidence angle of the light with respect to the sample surface plane was fixed at 10° with the s polarization. The XANES were collected in total electron yield (TEY) mode and the data were normalized to the incident photon flux. Notably, the TEY XANES data acquisition was most sensitive in the near surface area with a reliable probing depth of ~10nm. The XAS data at Cu and Zn K-edges were collected at the XAFS beamline (BL11.1 at the ELETTRA synchrotron). Notably, the Cu (8979eV) and Zn (9659eV) K-edges are ~700eV apart and the fine structure above the Cu absorption edge terminated before the appearance of the Zn edge. For simulating the data, for each spectrum a theoretical model was designed by adding shells around the central excited atom and least-square iterated the fitting parameters, namely the initial x-ray absorption energy at the edge (E_0), the radial distances (R) and the Debye–Waller type factors (σ^2 ($Å^2$)). The coordination numbers could be iterated too, but due to their strong correlation with σ^2 ($Å^2$)[6, 7] in the present study the coordination numbers were kept fixed at the preset values. Concerning the amplitude reduction factor (S_0^2), it could be found from a "standard" (data from a sample with well-known structure) and applied to a set of unknowns as a scale factor. In our case it has been fixed to the value obtained from fitting of the Fourier transformed XAFS spectrum of the pristine ZnO film and has been kept constant during the fitting of the ZnO:Cu based samples under different biasing states.

Notably, in addition to the *IV*, PL, and XAS measurements the samples were subjected to other types of characterizations including x-ray diffraction, scanning electron microscopy, secondary ion mass spectroscopy, Hall-effect measurement and ultra-violet visible measurement as elaborated in Section S1 of the Supplementary Materials. Moreover, specific details related to the XAS data collection and simulation are summarized in Section S2 of the Supplementary Materials. Further, some of the samples were annealed; in order to discriminate between Cu- and V_O-related contributions into the green luminescence, see Section S3 in the Supplementary Materials. Finally, we performed simulations of the electric field penetrating through the ZnO:Cu in the course of the HRS/LRS switching. The results of these simulations illustrated, even trivial but important for our discussion argument – that the field penetrated both beneath and laterally around Al contacts, see Section S4 in the Supplementary Materials.

2. Results

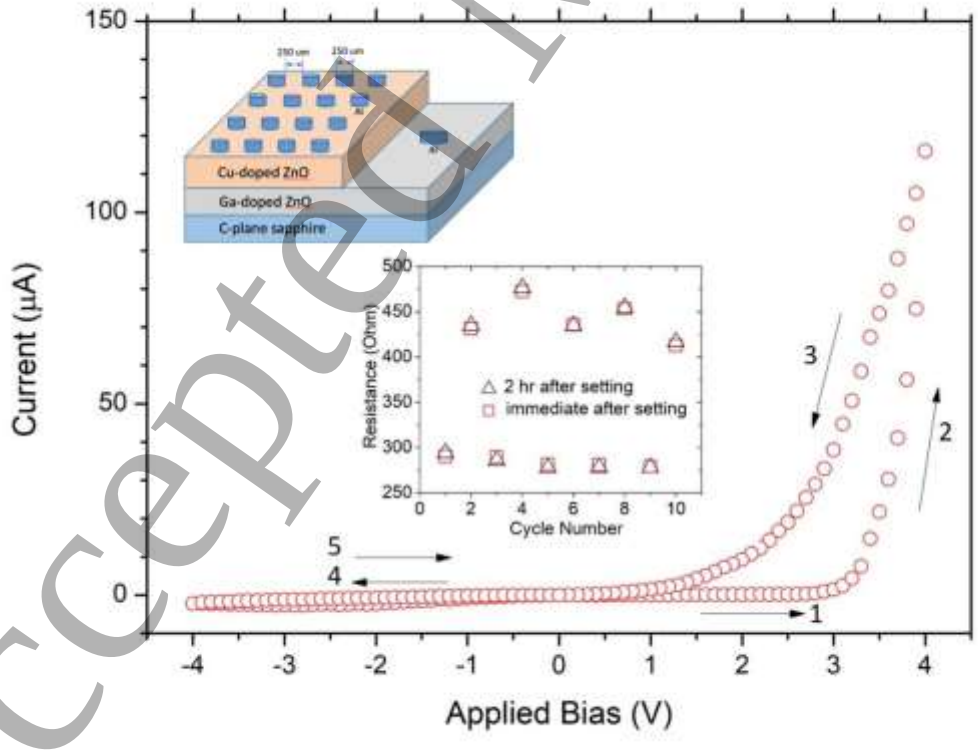

Figure 1: Typical IV data as collected from our samples indicating several prominent current intervals for the voltage loop of 0V→3V→4V→0V→-4V→0V. The insert in the center of

the panel shows LRS/HRS cycling test data by applying +4V/-4V and repeating the measurements in 2 hours after the bias was set. The inset in the upper left corner of the panel is the schematics of the Al/ZnO:Cu/ZnO:Ga/Al_2O_3 samples used in this study.

Figure 1 illustrates the resistive setting effect occurring in the Al/ZnO:Cu/ZnO:Ga/Al_2O_3 structures. As seen from Figure 1, at low positive voltages, i.e. 0V < $V_{applied}$ < +3V (stage 1 in Figure 1), the current remains low, meaning that the device is in the HRS. For +3V < $V_{applied}$ ≤ +4V (stage 2 in Figure 2), the current abruptly increased (reaching ~100 μA at +4 V), i.e. demonstrating switching to the LRS. Further, the current gradually decreased during the sweep down from +4 V to 0 V (stage 3 in Figure 2), however its magnitude remains somewhat higher as compared to that in the bias sweeping-up stage. Finally, applying the bias from 0 V to -4 V (stage 4 in Figure 1) and then sweeping it up from -4 V to 0 V (stage 5 in Figure 1) restores the system. Fitting the log(I) versus log($V_{applied}$) data for the positive bias showed the proportionalities of $I \sim V^{1.2}$ for 0 < $V_{applied}$ < 1V, $I \sim V^2$ for 1V < $V_{applied}$ < 2V, and $I \sim V^{4.5}$ for 3V < $V_{applied}$ < 4V, indicating that the mechanisms are governed by Ohm's law conduction, Child's law injection carriers and Poole-Frenkel emission, respectively.[8,11]

Importantly, the switching between HRS and LRS was observed in the course of multiple cycles as illustrated by the data in the inset to Figure 1. Firstly, we applied +4 V to set the sample to the LRS at ~270 Ω. After removing the set-bias, the monitoring *IV* measurements (with bias of +0.5 V which is smaller than the setting bias of 4V) confirmed that the LRS at ~270 Ω remained. Importantly, the LRS exhibited a long-term stability as proved by repeating the monitoring *IV* measurement 2 hours after the LRS setting (see the overlapping symbols for the first cycle in the inset to Figure 1). Secondly, we applied -4V to set the sample to the HRS at ~450 Ω. After removing the set-bias, the monitoring *IV* measurements confirmed that the HRS at ~450 Ω remained. Again, the HRS (and also the LRS) were remarkably stable as proved by repeating the monitoring *IV* measurements 2 hours after the HRS and LRS settings (see the overlapping symbols for the second cycle in the inset to Figure 1). Further cycling – see the

data in the inset to Figure 1 – confirmed the non-volatile HRS/LRS operation.[12] Notably, all Al/ZnO:Cu/ZnO:Ga components were tested individually, showing very similar resistive switching magnitude in multiple tests; the same performance was observed if switching the 4x4 device array as a whole.

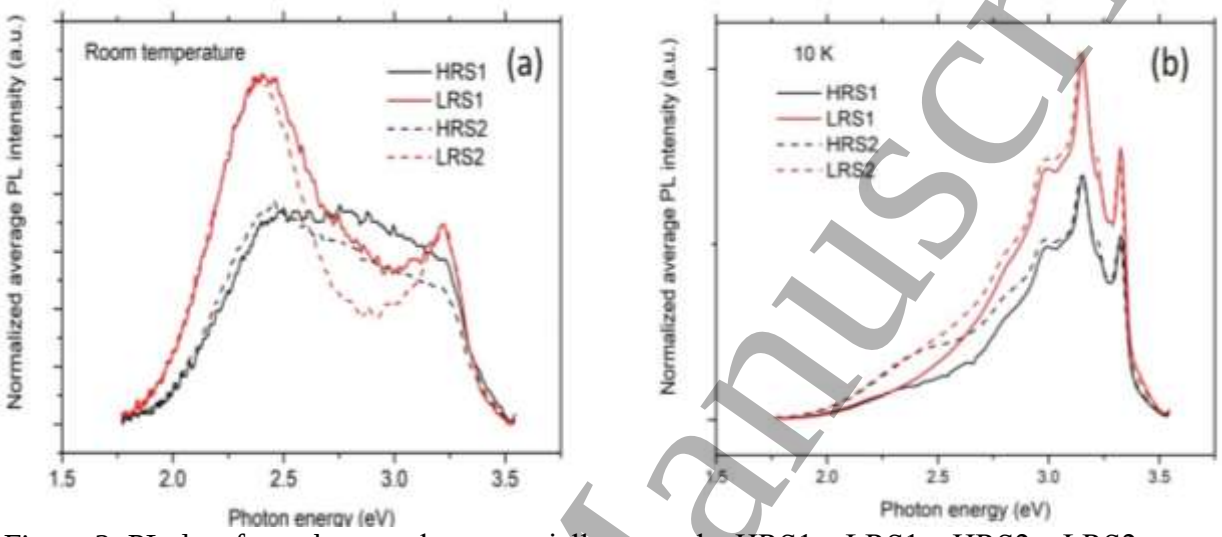

Figure 2: PL data from the sample sequentially set at the HRS1→LRS1→HRS2→LRS2 non-volatile memristor conditions as collected at (a) room temperature and (b) 10K; the data in both panels reveal a prominent PL modulation trend. Naturally, the raw PL intensity data at 10K were significantly higher than that that at room temperature and the normalization was applied to visualize the modulation trend.

The PL was measured on the samples front side subjected to the HRS/LRS cycles as explained above, and **Figure 2** shows the corresponding PL spectra. At the beginning, the sample was first set to the HRS conditions, labeling this state HRS1, and using it for the initial PL data collection, see Figure 2. The room temperature PL data reveal a broad spectrum extending from ~1.8 eV to ~3.4 eV without prominent features, see Figure 2(a). Further, the sample was switched to the LRS, labeling this state LRS1. Intriguingly, the room temperature PL demonstrated a prominent evolution while switching from the HRS1 to LRS1. Indeed, two new distinct features were observed: the intensive green luminescence emission peaking at 2.40 eV and the near band edge emission peaking at 3.22 eV. Further, the measurements were repeated in cycles and showed excellent reproducibility, e.g. see the black and red dotted lines

in Figure 2(a) corresponding to the data for the second cycle, i.e. HRS2 and LRS2, respectively. Thus, already accounting to the room temperature PL data, see Figure 2(a), we observed the luminescence modulation induced by the non-volatile resistive switching in our samples. Moreover, 10K PL data were collected in a similar manner, see Figure 2(b), also confirming the luminescence modulation. Indeed, even though the spectra in Figure 2(b) exhibit similar features (several near band edge emission peaks, e.g. at 3.02 eV, 3.16 eV, 3,23 eV and 3.33 eV, as well as a weaker green luminescence shoulder at 2.3 - 2.4 eV), the intensity of the near band edge emission peaks was prominently modulated. Importantly, the monitoring *IV* measurements were performed after completing each step of the PL data collection ensuring that the samples remained in the corresponding resistive states during the measurements. Overall, the spectral features in Figure 2 are in agreement with what is expected for the PL in ZnO.[13] Moreover, we interpret that the PL data collected from the near surface volume of the ZnO:Cu film only, since the laser excitation rapidly absorbs while entering the sample. Importantly, all 4x4 components of the device were set consequently at HRS/LRS to record the corresponding PL modulations.

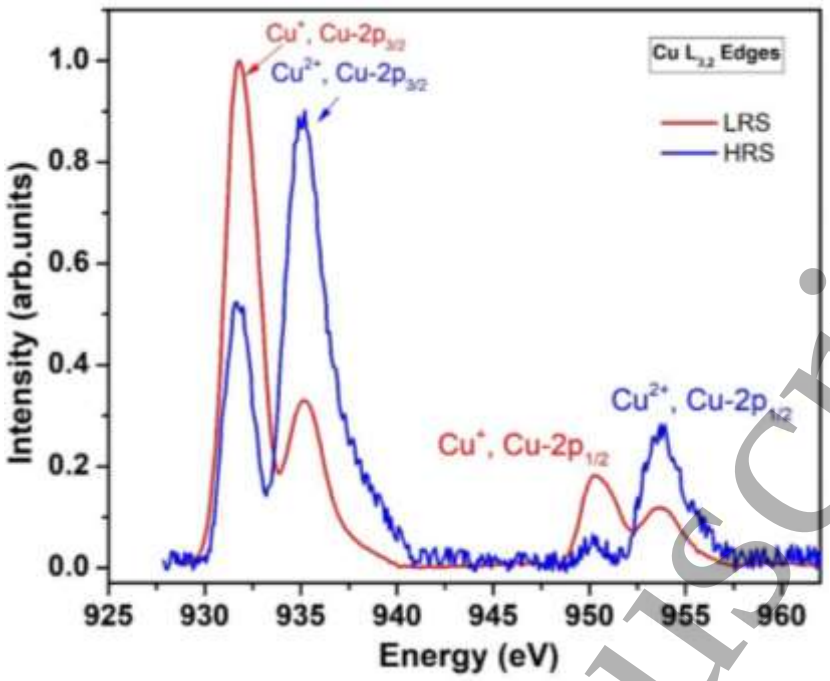

Figure 3: The Cu-$L_{3,2}$ edge XANES spectra as collected from the sample set firstly at HRS and consequently at LRS, showing the correlation between the resistive switching and Cu^{+} versus Cu^{2+} charge state abundance.

Figure 3 shows the Cu-$L_{3,2}$ edge XANES spectra for the samples set at HRS and LRS conditions, as such correlating with the HRS/LRS cycling measurements in Figure 1 and 2. Two pairs of peaks were observed in Cu-$L_{3,2}$ edge XANES spectra, namely the (932 eV, 935 eV) and the (950 eV, 954 eV). Importantly, similar pairs of peaks were observed in CuO and Cu_2O and correlated with the Cu^{2+} and Cu^{+} charge states, respectively.[14] Thus, the peaks in Figure 3 are assigned to the Cu^{2+} and Cu^{+} charge states of Cu in the near surface volume of the ZnO:Cu film. More specifically, the (932 eV, 935 eV) peaks correspond to (Cu^{+}, Cu^{2+}) associated with Cu-$2p_{3/2}$ and the (950 eV, 954 eV) peaks correspond to (Cu^{+}, Cu^{2+}) associated with Cu-$2p_{1/2}$, as also illustrated in Figure 3. However, most remarkably, the data in Figure 3 reveal prominent flips in Cu^{+}/Cu^{2+} occupations in ZnO:Cu film as a function of the resistive switching. For example, comparing the integral areas below the Cu^{+} and Cu^{2+} peaks, the relative Cu^{+} intensities are 26 % and 71 % for HRS and LRS, respectively. The observation in Figure 3 is in excellent correlation with the results in Figure 1 and 2 assuming all of the phenomena – resistive switching, luminescence modulation, and the Cu^{2+} versus Cu^{+} charge state alternation

– are occurring in the ZnO:Cu film. Importantly, the monitoring *IV* measurements were performed after completing each step of the XANES data collection ensuring that the samples remained in the corresponding resistive states during the measurements.

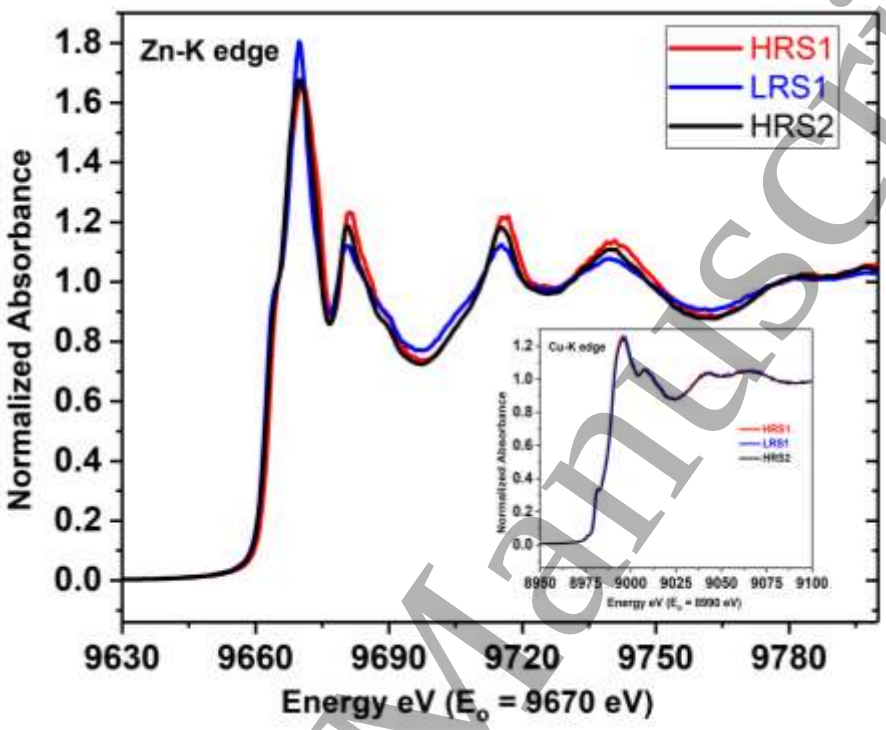

Figure 4: The normalized XANES spectra of Zn K-edge spectra as collected from the sample set consequently at HRS1, LRS1 and HRS2. The inset shows the corresponding Cu K-edge data.

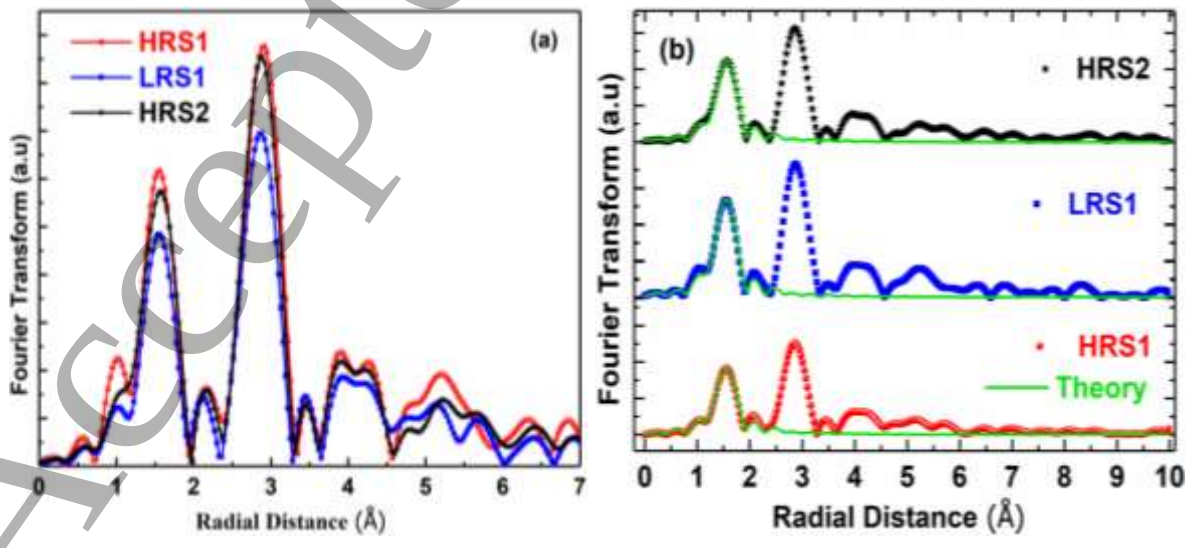

Figure 5. Fourier transforms of the data in Figure 4, (a) the raw data and (b) comparison of the experimental data (symbols) with a theoretical model (green solid lines).

Thus, assuming that the relevant transformations occur in the ZnO:Cu film we decided to investigate the microscopic arrangements in this material in more details. Consequently, **Figure 4** shows the normalized XANES spectra for Zn K-edge for the sample set at HRS1, LRS1 and HRS2 conditions consequently, while the inset shows the corresponding data for Cu K-edge. The data in Figure 4 were obtained by subtracting the smooth pre-edge background from the experimental spectra and taking the edge jump height as unity. Further details of the normalization procedure can be found elsewhere.[15] Notably, even though some discrepancy in the Zn K-edge data were observed, the direct analysis of the data in Figure 4 was not fully reliable and in order to enhance the accuracy, the Fourier transformation analysis was applied – see **Figure 5**. Importantly, the monitoring *IV* measurements were performed after completing each step of the XAFS data collection ensuring that the samples remained in the corresponding resistive states during the measurements.

Figure 5(a) shows the comparison of the Fourier transforms of the Zn K-edge spectra for the sample set consequently at HRS1, LRS1 and HRS2. Taking in to account the most prominent features in Figure 5(a), the peak appearing at ~1.5 Å is due to the first shell of the oxygen atoms and is related to the Zn-O bond distance. The second prominent peak at ~2.9 Å is associated with the second shell of Zn-Zn and Zn-O, and also multiple scattering. It is evident from Figure 5(a) that the intensity of these two peaks decreases when the sample is switched from the HRS1 to the LRS1. Moreover, the peaks amplitude is restored with returning to the HRS2 conditions.

Table I. Best fitting parameters for the simulations presented in Figure 5(b) considering the first Zn-O shell with a pre-set coordination number of 4 and the amplitude reduction factor (S_0^2) of 0.9. The σ^2 [Å^2] is the Debye-Waller factor, and R [Å] is the Zn-O bond distance.

	S_O^2	σ^2 [Å^2]	R [Å]
Pristine ZnO	0.9	0.0052 ± 0.0013	1.9714 ± 0.015
HRS1	0.9	0.0010 ± 0.0013	1.9719 ± 0.013
LRS1	0.9	0.0047 ± 0.0014	1.9725 ± 0.015
HRS2	0.9	0.0012 ± 0.0010	1.9810 ± 0.011

Further, the peak at ~1.5 Å includes only contribution from the first shell of the oxygen atoms, while the contributions from Zn-Zn, Zn-O (from the second shell) and multiple scattering are negligible. Therefore, for the Zn K-edge, the fits were performed in the range of 1–2 Å including the single scattering from the first shell of oxygen atoms only. Figure 5(b) shows the data and the fitted curves for the HR1-LRS1-HRS2 set of samples. The fitted parameters are listed in **Table I**, see the section describing the experimental methods for the fitting procedure details. The fitted Debye-Waller factors (labeled as σ^2 [Å^2] in Table I) increases from $1.0\pm1.3 \times 10^{-3}$ Å^2 to $4.7\pm1.4 \times 10^{-3}$ Å^2 as the sample is switched from HRS1 to LRS1, and then, upon switching to HRS2, deceases back to a lower value of $1.2\pm1.0 \times 10^{-3}$ Å^2. In the first approximation, this result indicates a higher degree of disorder for the Zn-O interatomic distance interlinked to the increase in the oxygen vacancy concentration in the LRS conditions.

Thus, one scenario is that by applying the positive bias and setting the structure at the LRS, the oxygen lean conditions are established, provoking the generation of the oxygen vacancies (V_O) at least in the vicinity of the ZnO:Cu surface. Concurrently, the crystalline structure of the material remains the same as confirmed by very similar R values as a result of the fits, see Table I, indicating none or negligible changes in the first shell interatomic Zn-O distance. Notably, the deviation of the fitted curves and experimental data for bigger distances in Figure 5(b) is an artefact since the fitting for longer distances was outside of the model capabilities.

3. Discussion

The non-volatile switching between HRS and LRS by respectively applying +4 V and – 4 V as observed in the current study is similar to the phenomenon called resistive switching. The models explaining the resistive switching phenomena could be classified in terms of two major categories: the conducting filament and the interface models. Notably, for the conducting filament mechanism to occur, the application of the unipolar bias is typically sufficient. Meanwhile, the *IV* characteristics in Figure 1, exhibit a bipolar switching behavior. In literature, this type of behavior is typically attributed to the interface conduction path model.[16 -19] Thus, already this general argument indicates that the modulations observed in Figure 1-5 may be associated with the modification of the ZnO:Cu near surface region. For example, in accordance with one of such models, in metal-ZnO based memristors, the V_O^+ move away from the Schottky type metal-semiconductor interface under negative bias (i.e. by directing the electric field into the bulk of the sample), widening the depletion width and resulting in the HRS.[16] Changing to the positive bias switches the V_O^+ drift, narrows the depletion region and, consequently, engages the electron injection resulting in the LRS.[16] Importantly, the hypothesis of the V_O drift in the near surface region of the ZnO:Cu film is consistent with the Zn-Zn and Zn-O bond fingerprints modulations, as observed in Figure 5.

Moreover, Figure 3 revealed prominent flips in Cu^+/Cu^{2+} occupations in ZnO:Cu film as a function of the resistive states; specifically, the Cu^+ abundance at the LRS was significantly higher than that at the HRS. In ZnO, the transition between the Cu^+ ($3d^{10}$) and Cu^{2+} ($3d^9$) is associated with the deep acceptor level Cu^{2+}/Cu^+ (0/-) located at E_A~200 meV below the conduction band minimum (CBM).[20-22] Accounting for a classical formalism, the relative concentration ratio is given by: $[Cu^{2+}]/[Cu^{+}] = g\ exp[-(E_F - E_A/kT)]$, where g is the degeneracy factor of the Cu acceptor in ZnO and E_F is the Fermi level position. Thus, accounting for $[Cu^{2+}]/[Cu^{+}]$ as measured in Figure 3, g=4, and kT=0.026 eV, we can make an estimate for E_F-E_A as a result of the HRS/LRS switching. Indeed, E_F-E_A may change by some

~ 30 meV, implying the E_F shift towards the CBM for the LRS. This is consistent with increasing the electron concentration in the conduction band for the LRS too.

Thus, based on the arguments above, our hypothesis is that the LRS is associated with establishing the oxygen lean conditions, with the elevation of the E_F toward the CBM and the higher Cu^+/Cu^{2+} occupation in the vicinity of the ZnO:Cu surface; below we use this hypothesis to explain the luminescence modulations.

Indeed, considering the green luminescence modulation first, there are literature arguments to relate it to Cu,[21-24] V_O[25-28] and zinc vacancies (V_{Zn}).[27, 29] Accounting for the role of Cu, the ionized Cu^+ acceptor ($3d^{10}$) captures a hole from the neighboring oxygen forming the excited state (Cu^+,h).[30] The (Cu^+,h) state transits to the Cu^{2+} ground state (i.e. Cu^{2+} ($3d^9$)) with the emission of a green photon. In its turn, Cu^{2+} captures an electron and recycles to the Cu^+ state. Assuming this mechanism works, the probability for the (Cu^+,h) → Cu^{2+} radiative transition depends on the abundance of Cu^+, so that the HRS/LRS switching modulates the green luminescence as seen in Figure 2(a), consistently with Figure 3. Alternatively, the V_O-related donor levels, e.g. negative-U donor state having zero phonon energy of 2.9 eV,[28] may be responsible for the green luminescence modulation too, because of the increasing electron occupancy at the donor states with the E_F moving towards the CBM at the LRS. Moreover, the increase of V_O concentration nearly the ZnO:Cu surface revealed by the Zn K-edge spectroscopy correlated with LRS would also enhance the GL. However, it is less likely to associate the green luminescence modulations with V_{Zn} exhibiting two acceptor levels at the lower half of the band gap,[31] because the E_F shifts – as deduced from the data in Figure 3 – will not affect the V_{Zn}-related acceptor states. For clarity, the corresponding Cu- and V_O-related transitions are illustrated in Fig.S1 in Sec.S3 in Supplementary materials).

Further discrimination between two realistic origins for the green luminescence modulation - V_O or Cu – may be possible by taking into account the data in Fig.S2 (see Sec.S3 in Supplementary materials). Indeed, these data illustrate the evolution of the green

luminescence parts of the PL spectra in ZnO:Cu upon annealing (NB, in a similar wafer, without the top Al array contacts). Upon anneals, the spectra in Fig.S2 unveil characteristic fine structures. Such fine structures used to be correlated with Cu [23], and not with V_O. Importantly, for the as-grown sample, the fine structure is not apparent, see Fig.S2. Thus, already this discrepancy indicates different contributions from the transitions illustrated in Fig.S1 into the green luminescence. Further, the PL peaks of the annealed samples are shifted towards higher energy, as compared to the as-grown sample (refer to its peak position marked with a dashed line in Fig.S2). Thus, accounting both for the fine structure and for the energy shift occurring in the annealed samples in Fig.S2, we interlink the green luminescence in these samples with Cu. In its turn, we assume that the peak centered at 2.40 eV in the as-grown sample – is the V_O signature, or at least dominated by the corresponding transitions. Thus, the arguments above suggest V_O to be a prime candidate to be responsible for the green luminescence modulation in Fig.2 (a).

Further, considering the near band edge emission, the peaks at 3.36 eV 3.33 eV, 3.23 eV, 3.16 eV, and 3.09 eV in Figure 2(b) are directly comparable with literature data for undoped ZnO grown by PLD.[32] Indeed, peaks at 3.36 eV, 3.33 eV, 3.23 eV, 3.16 eV and 3.09 eV were observed and attributed to the neutral donor bound exciton (D^0X), the two electron satellite (TES) of the D^0X, the donor-acceptor-pair (DAP), the first phonon replica of DAP (1LO DAP) and the second phonon replica of DAP (2LO DAP), respectively.[32] As such, we do a corresponding identification of the peaks in Figure 2(b) and conclude that these peaks are associated with the residual donors and acceptors in the samples rather than by the Cu-doping. Most importantly, shifting the E_F by the HRS/LRS switching will imply a corresponding change in the fraction of the neutral donors (D^0) in respect with the ionized donors (D^+ abundance) resulting in the NBE modulation in Figure 2(b).

Importantly, the data shown in Figure 2-5 were collected from the front side of the samples, so that the Al front-side electrodes prevented the analysis of the ZnO:Cu directly

underneath. Instead, the reconstructions occurred at the areas in between of the metallic contacts, providing exciting possibilities for the device applications. Indeed, in accordance with our simulations (see Section S4), the electric field penetrates into the region between the contacts when the set voltage is applied, correlating with the data in Figures 2-5. Worthy to mention that on the same sample structure Younas et al [8] observed modulation of saturated magnetization, which was associated to the change of the Cu^{+}/Cu^{2+} occupancy. Combining the present observations with literature data, we generalize that the ZnO:Cu films have potential to exhibit functionality inter-connecting electrical, optical and magnetic phenomenon via changing the Fermi level and thus the occupancy of V_O defect and Cu impurity.

4. Conclusions

In conclusion, we observed reversible correlated modulations in PL intensity, Cu^{+}/Cu^{2+} ratio revealed by XANES measurement and Zn-O bond fingerprints extracted from the Zn K-edge XAFS study induced by resistive switching in ZnO:Cu based memristors. With the resistive state switched from HRS to LRS and the PL intensity increased, the correlated increase in Cu^{+} occupancy implied the rise of the Fermi level toward the CBM. The rise of the Fermi level would correlate with the increase in electron occupancy of donor states (like $V_O(2+/0)$) in the band gap. The modulations of the PL intensity is due to the increases of the electron occupied luminescence origin states; for the green luminescence in terms of the Cu^{+} and/or V_O^0 and for the near band edge emission in terms of the residual donors. Importantly, the reconstructions as measured in the present study occurred even outside of the areas of the front side metallic contacts, providing exciting possibilities for the functionalization.

Acknowledgements

This work was financially supported by the HKSAR RGC GRF (17302115). The collaboration with the University of Oslo was enabled by the INTPART Program at the Research Council of Norway (grant nr 261574). We acknowledge the support of Elettra Sincrotrone (Trieste, Italy) for the provision of beam time and ICTP-Elettra Users Programme for a financial grant. We are thankful to Pakistan Atomic Energy Commission for supporting this work.

References

[1] P. M. Pattison, J. Y. Tsao, G. C. Brainard & B. Bugbee, Nature 563, 493(2018)

[2] C. v. Dewitz, F. Hatami, M. Millot, J. M. Broto, J. Léotin, and W. T. Masselink, Appl. Phys. Lett. 95, 151105 (2009)

[3] YC Yang, F. Pan F, F. Zeng F, M. Liu M. Journal of Applied Physics, 106, 123705(2009)

[4] J. Xiao, T.S. Herng, J. Ding J, K.Zeng, Journal of Alloys and Compounds 709, 535(2017)

[5] T. Wang, HP Ma, JG Yang, JT Zhu, H. Zhang, J.Feng, SJ Ding, HL Lu HL, DW Zhang Journal of Alloys and Compounds, 744 381(2018).

[6] AS Sokolov, H Abbas, Y Abbas, C Choi, Journal of Semiconductors. 42 13101(2021)

[7] M. Kund, G. Beitel, C. Pinnow, T. Rohr, J. Schumann, R. Symanczyk, K. Ufert, G. Muller, IEDM Technical Digest., Dec 5, 754 (2005).

[8] M. Younas, C. Xu, M. Arshad, L.P. Ho, S. Zhou, F. Azad, M.J. Akhtar, S. Su, W. Azeem, F.C.C. Ling, ACS Omega, 2 8810 (2017)

[9] C. He, J. Li, X. Wu, P. Chen, J. Zhao, K. Yin, M. Cheng, W. Yang, G. Xie, D. Wang, D. Liu, R. Yang, D. Shi, Z. Li, L. Sun, G. Zhang, Adv Mater, 25, 5593(2013)

[10] X. Yang, C. Shan, Q. Liu, M. Jiang, Y. Lu, X. Xie, B. Li, D. Shen, ACS Photonics, 5, 1006(2017)

[11] M. Younas, J. Shen, M. He, R. Lortz, F. Azad, M.J. Akhtar, A. Maqsood, F.C.C. Ling, RSC Advances, 5, 55648(2015)

[12] In practice, the LRS and HRS stability lasted considerably longer as confirmed by the post-PL and post-XAS controlling tests.

[13] T.Moe Børseth, B.G. Svensson, and A. Yu. Kuznetsov, P. Klason, Q. X. Zhao, and M. Willander, Appl. Phys. Lett. 89, 262112 (2006)

[14] J. Sohn, S.-H. Song, D.-W. Nam, I.-T. Cho, E.-S. Cho, J.-H. Lee, H.-I. Kwon, Semiconductor Science and Technology, 28 (2013).

[15] J. Wong, F.W. Lyte, R. P. Messmer and D. H. Maylotte, Phys. Rev. B, 30, 5596 (1984)

[16] H.Y. Peng, G.P. Li, J.Y. Ye, Z.P. Wei, Z. Zhang, D.D. Wang, G.Z. Xing, T. Wu, Applied Physics Letters, 96 (2010)

[17] F.P. Yu Chao Yang, Qi Liu, Ming Liu, Fei Zeng, ACS Nano Letters, 9 1637(2009)

[18] J.Y. Chen, C.L. Hsin, C.W. Huang, C.H. Chiu, Y.T. Huang, S.J. Lin, W.W. Wu, L.J. Chen, Nano letters, 13 3671(2013).

[19] J.S. Choi, J.S. Kim, I.R. Hwang, S.H. Hong, S.H. Jeon, S.O. Kang, B.H. Park, D.C. Kim, M.J. Lee, S. Seo, Applied Physics Letters, 95 22109(2009).

[20] F.A. Selim, M.C. Tarun, D.E. Wall, L.A. Boatner, M.D. McCluskey, Applied Physics Letters, 99 202109(2011).

[21] M.D. McCluskey, S.J. Jokela, Journal of Applied Physics, 106 071101(2009).

[22] C. G. Rodriguez, *Relationship between structure and magnetic beahviour in ZnO-based systems*, Springer International, Switzerland, 2015

[23] R. Dingle, Physical Review Letters, 23 579(1969).

[24] G.Q.L. S. L. Shi, S. J. Xu, Y. Zhao, G. H. Chen, Journal of Physical Chemistry B, 110 10475(2006).

[25] K. Vanheusden, W.L. Warren, C.H. Seager, D.R. Tallant, J.A. Voigt, B.E. Gnade, Journal of Applied Physics, 79 7983(1996).

[26] S.A. Studenikin, N. Golego, M. Cocivera, Journal of Applied Physics, 84 2287(1998).

[27] C. Ton-That, L. Weston, M.R. Phillips, Physical Review B, 86 115205(2012).

[28] D.M. Hofmann, D. Pfisterer, J. Sann, B.K. Meyer, R. Tena-Zaera, V. Munoz-Sanjose, T. Frank, G. Pensl, Applied Physics A, 88 147(2007).

[29] Y.W. Heo, D.P. Norton, S.J. Pearton, Journal of Applied Physics, 98 73502(2005).

[30] N.-u. Rehman, M. Mehmood, R. Rizwan, M.A. Rasheed, F.C.C. Ling, M. Younas, Chemical Physics Letters, 609 26(2014).

[31] A. Janotti, C.G. Van de Walle, Physical Review B, 76 165202(2007).

[32] Z. Wang, S.C. Su, M. Younas, F.C.C. Ling, W. Anwand, A. Wagner, RSC Advances, 5 12530(2015).